scientific reports

OPEN

Electromagnetic field produced by radiation source submerged in non-homogeneous seawater

Honglei Wang[1,2✉], Yingda Ren[1,2] & Kunde Yang[1,2,3]

Electromagnetic (EM) waves are one of the important carriers for information exchange in seawater. The EM parameters of seawater are important factors that affect the performance of EM wave propagation. In the real marine environment, non-constant EM parameters make it impossible to consider seawater as a homogeneous media in the model. However, there are few targeted analyses in the existing studies. In this paper, an N-layered media model was established to investigate the influence of non-constant EM parameters on EM wave propagation in seawater. A direct global matrix method is proposed to solve the EM fields, whose result accuracy does not decrease with the increasing number of layers. The necessity and correctness of the model and methods are verified through numerical simulations and sea experiments. Combined with the existing marine environment database, the propagation characteristics of EM waves in different EM parameter profiles of seawater were analyzed through numerical experiments. The results indicated that the non-homogeneous seawater has a great impact on the intensity, phase, change rate, and spatial distribution of EM waves. Furthermore, the influence is not only reflected in the underwater EM field but also in the air and increases with frequency.

The propagation of electromagnetic (EM) waves in stratified media has been the subject of investigation for many years since Sommerfeld's classic work. Due to the development of explorations and exploitations in the ocean in recent years, applications using EM waves have drawn a significant amount of attention, including underwater detection, remote sensing, marine environment monitoring, and underwater communications[1–4]. However, in the actual marine environment, the non-homogeneous nature of seawater affects the propagation performance of EM waves in these applications. This paper presents some interesting results and valuable conclusions when seawater is considered a non-homogeneous media.

There have been some studies on underwater EM wave propagation in recent years. The simple three-layered media model of seabed-seawater-air was established[5–7]. And it was recognized in these papers that underwater EM waves can achieve propagation distances beyond skin depth through lateral waves. Marine experiments and simulation verification were carried out[8], and the frequency response curves between 10 kHz and 1 MHz for different distances have been provided. Smolyaninov et al. found through experiments that 2.4 GHz EM waves can propagate more than 15 cm in seawater, which indeed exceeds the skin depth (3 mm)[9]. They believe that these are due to the existence of lateral waves. Besides, Xu et al. deduced and simulated the approximate formula of the EM field generated by the horizontal electric dipole under the two-layer model (air-seawater, seawater-seafloor)[10]. EM fields in air produced by underwater magnetic dipoles with varying attitudes are investigated[11]. The underwater EM wave propagation models including the non-uniform seafloor are established and analyzed[12]. Nie et al.[13] analyzed the generation mechanism of lateral waves along the seabed based on GH shift. And the propagation characteristics were verified and analyzed through experiments, which is helpful to realize underwater wireless sensor networks on the seabed[14]. However, seawater is regarded as a medium with constant EM parameters in these studies, which is quite different from the actual environment.

Affected by temperature, salinity and pressure, the EM parameters of seawater in the actual marine environment change with time and space. Models of permittivity in seawater at different frequencies were demonstrated[15,16]. The measurements were carried out to obtain the permittivity of Dead Sea water[17]. The spatial and seasonal variability of real and imaginary parts of Persian Gulf permittivity at the C-band is computed by a numerical model and an experimental model[18]. Besides, the conductivity in seawater can be calculated from

[1]School of Marine Science and Technology, Northwestern Polytechnical University, Xi'an 710072, China. [2]Key Laboratory of Ocean Acoustics and Sensing, Ministry of Industry and Information Technology, Northwestern Polytechnical University, Xi'an 710072, China. [3]Ocean Institute of Northwestern Polytechnical University, Taicang 215400, China. ✉email: wanghonglei@nwpu.edu.cn

marine environment data based on an international standard, which is the Thermodynamical Equation of Seawater-2010 (TEOS-10)[19]. Statistics of spatial and temporal changes in average conductivity are presented[20]. The vertical distribution of seawater conductivity was analyzed, and the results show that a high linear correlation exists between temperature and conductivity[21].

Some studies have been carried out on the influence of EM parameters on the propagation of EM waves in seawater. The attenuation loss of EM waves propagating in seawater at different seawater conductivities was simulated and obtained[22,23]. Saini et al.[24] calculated the conductivity based on salinity and temperature and compared the propagation attenuation in deep water and shallow water. Tahir et al.[25] presented that received power is linearly attenuated in seawater of lower conductivity, and the attenuation becomes exponential when the conductivity and frequency are high. Wang and Li[26] investigated the effects of seafloor conductivity on EM wave propagation above the shallow sea. The numerical results indicated that seafloor conductivity has less impact on EM field strength. The impact of non-homogeneous seawater on propagation characteristics was not studied in these studies.

In this paper, an N-layered media model is established based on the distribution characteristics of EM parameters. The direct global matrix approach is proposed to solve the EM field produced by a radiation source submerged in non-homogeneous seawater. Then, the necessity and correctness of the model and method are verified through numerical simulation and a sea experiment. Combined with the existing marine environment database, the impact of different EM parameter profiles on EM wave propagation is comparatively analyzed in Section "Comparison and verification". The final section concludes the paper.

Numerical modeling of EM fields

Compared with the vertical direction, the changes in the EM parameters of seawater in the horizontal direction are almost negligible within the same range[20]. Therefore, the non-homogeneous seawater in this paper mainly considers the variations of EM parameters with seawater depth. The geometric structure of the N-layered media model incorporating seawater with non-constant EM parameters is established in Fig. 1. In this model, the first layer and Nth layer are conceptualized as semi-infinite half-spaces, representing the air and seabed respectively. These bounding layers are assumed to extend to infinity in the vertical directions. The media from the second to the $N-1$-th layers is seawater. In m-th layer ($m = 1, 2, \ldots, N$), the permittivity is ε_m, and the permeability and conductivity are μ_m and σ_m respectively. A horizontal magnetic dipole (HMD) with a magnetic moment of IS, where I is the current flowing in a loop of area S, is located in seawater at a depth of d. The origin O of the cylindrical coordinate system, which is the global coordinate system, is at the center of the HMD. In this section, a numerical model of EM wave propagation in non-homogeneous seawater is established, and a new solution method suitable for the multi-layer EM wave propagation model is introduced.

EM fields in any layer

The time harmonic factor of the EM field is set to $e^{-i\omega t}$ in this paper. The receiving point P is assumed to be located in layer m. Taking E_ρ and H_φ as an example, the EM field components in the frequency domain can be written as follows[27]:
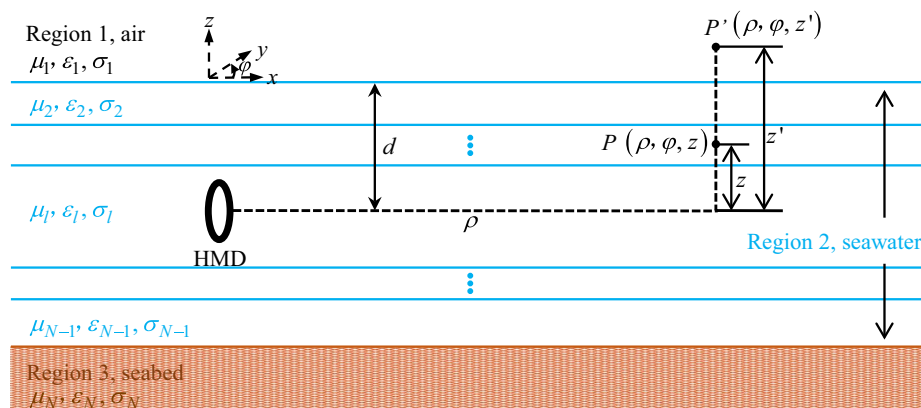

Figure 1. Geometrical configuration of the N-layered media model.

$$E_{m\rho} = \int_{-\infty}^{\infty} dk_\rho \frac{jk_{mz}}{k_\rho}(A_m e^{jk_{mz}z} - B_m e^{-jk_{mz}z})H_1^{(1)'}(k_\rho\rho)\sin(\varphi)$$

$$+ \int_{-\infty}^{\infty} dk_\rho \frac{-j\omega\mu_m}{k_\rho^2\rho}(C_m e^{jk_{mz}z} + D_m e^{-jk_{mz}z})H_1^{(1)}(k_\rho\rho)\sin(\varphi)$$

$$H_{m\varphi} = \int_{-\infty}^{\infty} dk_\rho \frac{-jk_{mz}}{k_\rho^2\rho}(C_m e^{jk_{mz}z} - D_m e^{-jk_{mz}z})H_1^{(1)}(k_\rho\rho)\sin(\varphi)$$

$$+ \int_{-\infty}^{\infty} dk_\rho \frac{j\omega\varepsilon'_m}{k_\rho}(A_m e^{jk_{mz}z} + B_m e^{-jk_{mz}z})H_1^{(1)'}(k_\rho\rho)\sin(\varphi)$$

(1)

where $k_{mz} = \sqrt{k_m^2 - k_\rho^2}$. $k_m = \sqrt{\omega^2\mu_m\varepsilon_m + j\omega\mu_m\sigma_m}$ is the propagation constant, which is directly related to the EM parameters of the media in layer m. k_ρ is the integrated variable, ω is the angular frequency of the EM wave. $\varepsilon'_m = \varepsilon_m + j\sigma_m/\omega$ is the complex permittivity. A_m, B_m, C_m and D_m denote amplitudes for TM and TE wave components. $H_1^{(1)}(k_\rho\rho)$ is the first order Hankel functions of the first kind, and the subscript and superscript correspond to its order and kind, respectively. $H_1^{(1)'}(k_\rho\rho)$ denotes the derivative of $H_1^{(1)}(\xi)$ with respect to its argument ξ. $E_{m\rho}$ represents the electric field component in the ρ direction (radial direction), and $H_{m\varphi}$ represents the magnetic field component in the φ direction (azimuthal direction) in the m-th layer.

As shown in Fig. 1, the boundary conditions at the interfaces require that tangential components of electric and magnetic fields are continuous for all ρ and φ, respectively. The following equations exist between the amplitude coefficients of the m-th and $m+1$-th layers. $B_1 = D_1 = A_N = C_N = 0$ in layer 1 and N because no waves come from infinity.

$$k_{mz}\left[A_m\phi_m^+ - B_m(\phi_m^+)^{-1}\right] = k_{(m+1)z}\left[A_{m+1}\phi_m^- - B_{m+1}(\phi_m^-)^{-1}\right]$$

$$\varepsilon_m\left[A_m\phi_m^+ + B_m(\phi_m^+)^{-1}\right] = \varepsilon_{(m+1)}\left[A_{m+1}\phi_m^- + B_{m+1}(\phi_m^-)^{-1}\right]$$

$$k_{mz}\left[C_m\phi_m^+ - D_m(\phi_m^+)^{-1}\right] = k_{(m+1)z}\left[C_{m+1}\phi_m^- - D_{m+1}(\phi_m^-)^{-1}\right]$$

$$\mu_m\left[C_m\phi_m^+ + D_m(\phi_m^+)^{-1}\right] = \mu_{(m+1)}\left[C_{m+1}\phi_m^- + D_{m+1}(\phi_m^-)^{-1}\right]$$

(2)

where $\phi_m^+ = e^{jk_{mz}d_m}$, $\phi_m^- = e^{jk_{(m+1)z}d_m}$.

The equation system obtained according to the boundary conditions is a homogeneous linear equation system. To obtain a non-zero solution for the amplitude coefficients, new equations need to be introduced. According to the antenna type, some new variables are introduced, i.e., A_l^+, B_l^+, E_{hmd}. The equations between amplitude coefficients in layer l, where the antenna is located, are as follows:

$$A_l^+ - A_l^- = B_l^- - B_l^+ = E_{hmd}$$

$$C_l^+ - C_l^- = D_l^+ - D_l^- = H_{hmd}$$

(3)

where $E_{hmd} = IS\omega\mu_l k_\rho^2/8\pi k_{lz}$, $H_{hmd} = -ISk_\rho^2/8\pi$. A_l^+, B_l^+, C_l^+ and D_l^+ are used for $z > 0$, and A_l^-, B_l^-, C_l^- and D_l^- are used for $z < 0$.

Combining Eqs. (2) and (3), the amplitude coefficients A_m, B_m, C_m and D_m in each layer can be obtained according to the boundary conditions and the excitation amplitude of the dipole configuration.

Direct global matrix approach

In the previous studies, the amplitude coefficients in each layer could be solved by the recursive propagation approach[26,28]. However, it was found in numerical experiments that as the number of layers in the model increases, the results gradually appear to be oscillating errors. This is especially obvious when the integrand parameter k_ρ is large. There are two reasons for this phenomenon. One is that there are errors in numerical calculations, which are caused by computer accuracy. The other is that when k_ρ is large, the parameters in the propagation matrix are greatly different. Since the number of recursions is positively correlated with the number of layers, the error gradually increases and affects the calculation of the EM field.

In order to avoid that the solution accuracy is affected by the number of layers in the model, a direct global matrix approach suitable for multi-layer EM wave models is proposed to solve the amplitude coefficients in each layer. A system of linear equations containing the all-unknown amplitude coefficients is established. Combining the boundary conditions and the excitation amplitude of the dipole configuration, its coefficient matrix can be obtained.

The origin position of the depth axis is quite critical for numerical stability and calculation error. If the layer is very thick or the horizontal wavenumber is large, i.e., $k_{mz}d_m \gg 1$, some coefficients in the matrix are easily overlooked in numerical analysis. In the direct global matrix approach, these problems can be easily avoided by changing the local coordinate origin of layer m[29]. The local coordinate system in the m-th layer is shown in Fig. 3. The coordinates at the receiving point satisfy the following:
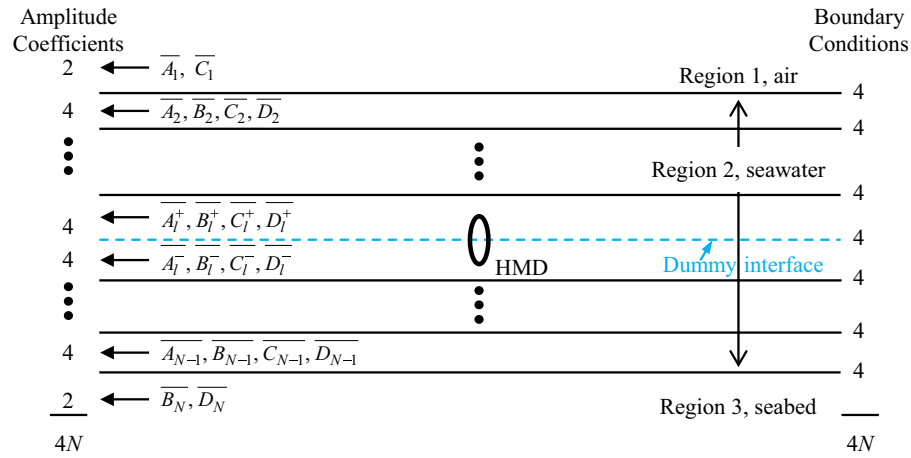
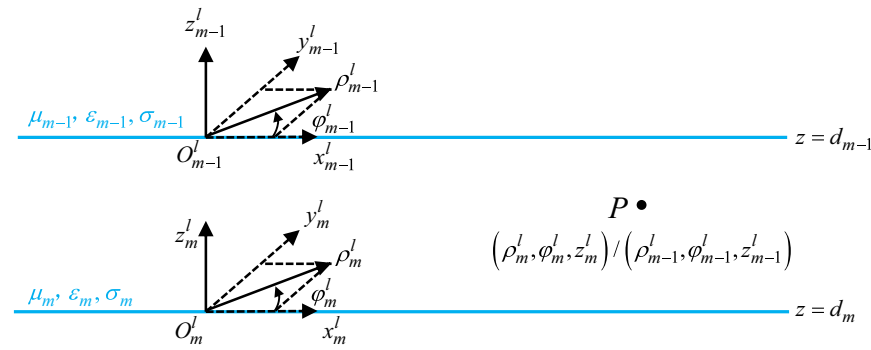**Figure 2.** Amplitude coefficients and boundary conditions in N-layered media model.

Figure 3. Local coordinate systems in layer m.

$$\begin{aligned} \rho_m^l &= \rho_{m-1}^l = \rho \\ \varphi_m^l &= \varphi_{m-1}^l = \varphi \\ z_m^l &= z - d_m \quad z_{m-1}^l = z - d_{m-1} \end{aligned} \tag{4}$$

where $(\rho_m^l, \varphi_m^l, z_m^l)$ is the coordinate of the receiving point in the local coordinate system with the origin at $z = d_m$. $(\rho_m^l, \varphi_m^l, z_m^l)$ is the coordinate in the local coordinate system with the origin at $z = d_{m-1}$.

In the local coordinate system, the linear equations to solve the amplitude coefficients of layer m-th and $m + 1$-th are as follows:

$$\left[\mathbf{U}_m^\chi \ \mathbf{L}_m^\chi \right] \left[\mathbf{X}_m^\chi \ \mathbf{X}_{m+1}^\chi \right]^T = \mathbf{0} \tag{5}$$

where $\chi = s$, p, which represent TE wave and TM wave respectively. $\mathbf{U}_m^\chi, \mathbf{L}_m^\chi, \mathbf{X}_m^\chi$ can be found in Appendix.

However, the relation formula for the amplitude coefficients in layer l-th is completely different from Eq. (5). In order to construct the global matrix, all equations of amplitude coefficients need to be forced to exhibit the same behavior. It is illustrated in Fig. 2 that the horizontal plane where the HMD is located is assumed to be a dummy interface[12]. The linear equations of amplitude coefficients at the dummy interface can be written as:

$$\left[\mathbf{U}_{TR}^\chi \ \mathbf{L}_{TR}^\chi \right] \left[\mathbf{XU}_l^\chi \ \mathbf{XL}_l^\chi \right]^T = \mathbf{b}^\chi \tag{6}$$

where $\mathbf{U}_{TR}^\chi, \mathbf{L}_{TR}^\chi, \mathbf{XU}_l^\chi, \mathbf{XL}_l^\chi$ and $\mathbf{b}^\chi$ can be found in Appendix.

Combining Eqs. (5) and (6), the system of linear equations containing all unknown amplitude coefficients in the model can be obtained as Eq. (7), where the coefficient matrix is a full-rank matrix. The amplitude coefficients in each layer can be obtained directly by solving the linear matrix, which avoids the expansion of errors.

$$
\begin{bmatrix}
\mathbf{U}_1^\chi & \mathbf{L}_1^\chi & & & & & & \\
 & \ddots & \ddots & & & & & \\
 & & \mathbf{U}_{l-1}^\chi & \mathbf{L}_{l-1}^\chi & & & & \\
 & & & \mathbf{U}_{TR}^\chi & \mathbf{L}_{TR}^\chi & & & \\
 & & & & \mathbf{U}_l^\chi & \mathbf{L}_l^\chi & & \\
 & & & & & \ddots & \ddots & \\
 & & & & & & \mathbf{U}_{N-1}^\chi & \mathbf{L}_{N-1}^\chi
\end{bmatrix}
\begin{bmatrix}
\mathbf{X}_1^\chi \\ \vdots \\ \mathbf{X}_{l-1}^\chi \\ \mathbf{X}\mathbf{U}_l^\chi \\ \mathbf{X}\mathbf{L}_l^\chi \\ \mathbf{X}_{l+1}^\chi \\ \vdots \\ \mathbf{X}_N^\chi
\end{bmatrix}
=
\begin{bmatrix}
\mathbf{0} \\ \vdots \\ \mathbf{0} \\ \mathbf{b}^\chi \\ \mathbf{0} \\ \vdots \\ \mathbf{0}
\end{bmatrix}
\tag{7}
$$

The amplitude coefficients in each layer can be obtained based on the solution results of Eq. (7), which can be substituted into Eq. (1). The Sommerfeld integral in Eq. (1) can be solved by the fast Fourier transform (FFT) approach, which has fast computational speed and high accuracy[30]. In this way, the EM field components at the receiving point can be obtained.

Comparison and verification

As shown in Fig. 4, in order to verify the necessity and correctness of the model and the direct global matrix approach in the previous section, numerical simulation and a sea experiment are designed and carried out in this section.

Numerical simulation

Taking the non-constant seawater conductivity in the vertical direction as an example, models with different numbers of seawater layers were established in the numerical model. The results are compared and analyzed in this subsection. Since the conductivity of the seawater mostly varies from 3 S/m to 5 S/m and is negatively correlated with depth in most sea areas, the conductivity profile and the number of layers in the seawater are set as shown in Fig. 5. And the conductivity of each layer is an average value. The remaining EM parameters of each layer in the model are shown in Table 1. The emission depth of underwater radiation source is 22 m. The height of the receiving point from the air-seawater interface is set to 10 m. The magnetic dipole moment $IS = 56.745 \text{A m}^2$, and the frequency $f = 10 \text{ kHz}$.

It is illustrated in Fig. 6a that as the number of layers increases, the value of $|B_1|$ calculated by the recursive propagation method gradually becomes larger. This is contrary to the initial condition $B_1 = 0$. When $k_p \leq -0.6$ or $k_p \geq 0.6$ in models with seawater layers of 5 and 10, $|A_1|$ has an oscillating error and is exponentially related to k_p as shown in Fig. 6b. However, all of these do not appear in Fig. 6c,d. The amplitude coefficients of TE wave are also similar. These errors greatly impact the accuracy of the EM field. Therefore, the recursive propagation method is not suitable for solving the EM field in the N-layered media model with large number of layers, and it is necessary to propose the direct global matrix approach.

The EM fields in the model with different seawater layers are calculated by the direct global matrix approach. Component H_φ is taken as examples to illustrate the comparison. Other electric and magnetic components have similar results. It is illustrated in Fig. 7 that when the horizontal distance is large, the intensity and phase of the received EM field components are negatively correlated with the number of layers in seawater. And the maximum difference in intensity under different layered models exceeds 9 dB. This finding highlights the influence of non-homogeneous seawater on EM wave propagation and the shortcoming of traditional model that
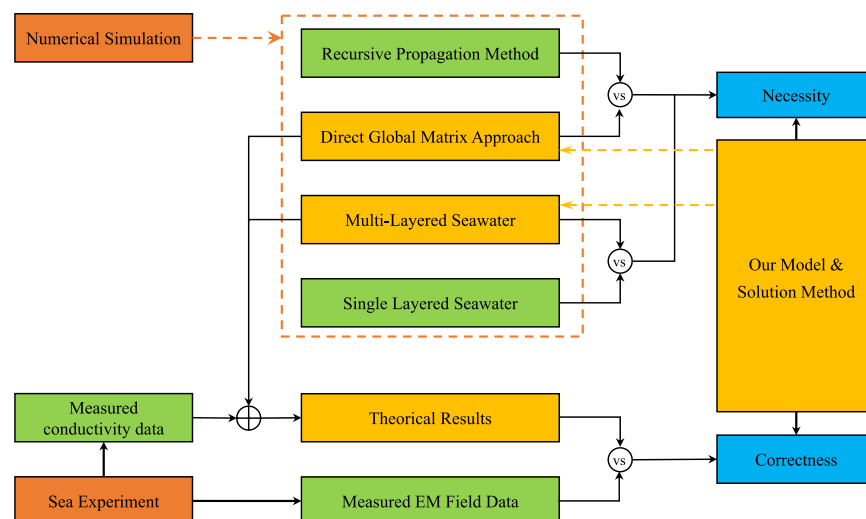

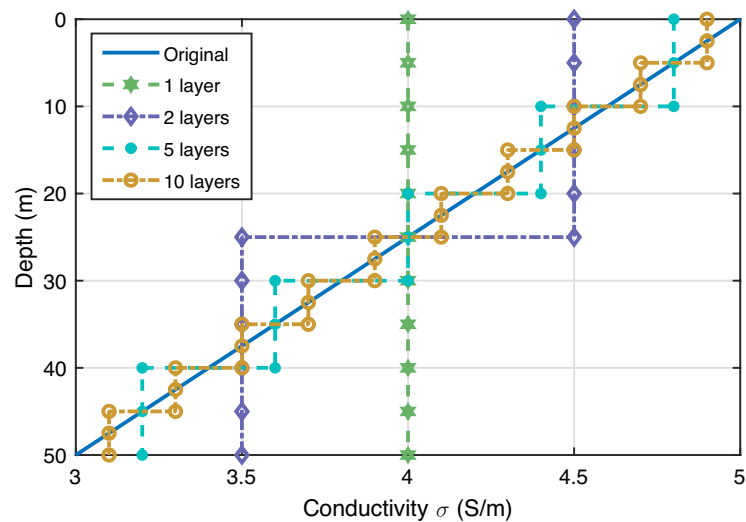**Figure 4.** Process for model and method validation.

Figure 5. Conductivity profile and the number of layers in seawater.

Layer serial number	1	2 − (N − 1)	N
Media type	Air	Seawater	Seabed
Permeability(H/m)	$4\pi \times 10^{-7}$	$4\pi \times 10^{-7}$	$4\pi \times 10^{-7}$
Conductivity(S/m)	0		0.04

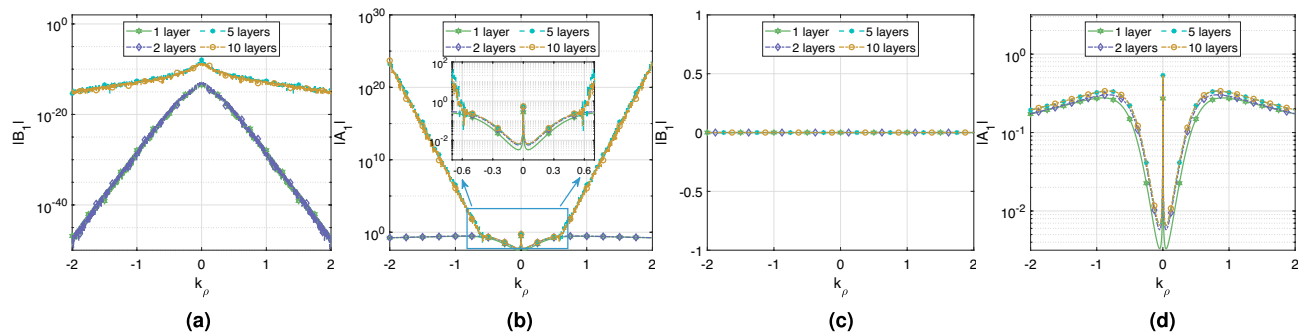**Table 1.** The EM parameters of each layer in the numerical simulation.

Figure 6. The amplitude coefficients of the TM wave in the N-layer model with different seawater layers. (**a**) $|B_1|$ calculated by recursive propagation method, (**b**) $|A_1|$ calculated by recursive propagation method, (**c**) $|B_1|$ calculated by direct global matrix approach, (**d**) $|A_1|$ calculated by direct global matrix approach.

simplify the non-homogeneous seawater as a single layer. When the horizontal distance is small, the intensity and phase have no obvious relationship with the number of layers. This is because the main energy in the EM field components comes from the direct wave, and the intensity is only related to the EM parameters of the seawater between the transceivers. The rate of the phase change also has a similar relationship with the intensity. As the number of seawater layers increases, the EM field components gradually become stable. These indicate that establishing an N-layer media model is necessary for investigating the impact of non-homogeneous seawater on EM wave propagation.

Sea experiment

A sea experiment was designed and carried out to verify the correctness of the solution method in the previous section. The seawater depth of the experimental area was about 20 m. The experiment system consists of an underwater transmitting antenna and a receiving antenna. Among them, the underwater transmitting loop antenna is designed to be 0.85 m in diameter. The receiving antenna is a ferrite-core loop antenna, which can convert the magnetic field into a voltage signal. In the experiment, the depth of the underwater transmitting antenna was 1m, the emission current was 1 A, the receiving antenna was placed 0.1m above and below the seawater-air surface sequentially, and the operating frequency was set to be 19 kHz.
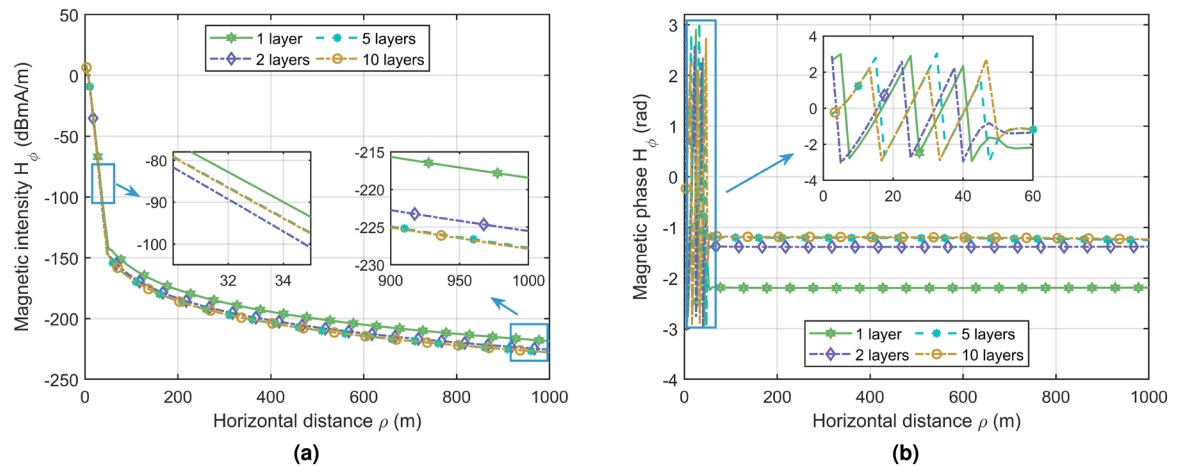
Figure 7. Variation of receiving EM field component H_φ under different seawater layers. (**a**) the intensity, (**b**) the phase.

It is illustrated in Fig. 8 that seawater conductivity measured by the conductivity-temperature-depth (CTD) system changes with depth. Throughout the experiment, the conductivity remained essentially constant over time. Since the experimental area is shallow and the experiment is carried out in winter, the change in seawater conductivity along the depth is only 0.9% in this experiment. According to CTD data from previous marine surveys, the change in seawater conductivity in the South China Sea reached 13% in the summer. In our future study, experiments about EM wave propagation in the South China Sea will be considered. According to the samples of CTD, the number of layers in the seawater region was set to be 30 in the model. The average conductivity of the experimental area was 4.55 S/m. The remaining EM parameters are the same as in Table 1.

The induced voltage of the receiving antenna in the experiment and the theoretical results are presented in Fig. 9. It is illustrated in Fig. 9 that there are certain fluctuations in the experimental data, which are due to the impact of waves on the attitude of the underwater antenna. But all the experimental data are basically consistent with the theoretical results, whether the receiving points are in air or seawater. The results show that the N-layered media model and method proposed in this paper are correct.

To sum up, the necessity of the direct global matrix approach and the N-layered media model was also verified by comparing the EM field components generated by HMD in seawater with non-constant conductivity under different layered models. In addition, we verified the correctness of the model and the method through a sea experiment in this section. However, both numerical simulation and sea experiments have certain limitations. For example, in the real-world marine environment, the conductivity profile of seawater is not as regular as in numerical simulation, exhibiting varying gradients throughout the entire profile. On the other hand, while invaluable for validating theoretical models and understanding practical implications, sea experiments are constrained by time, space, and environmental factors. The results obtained from sea experiments may not be representative of all sea areas. Moreover, due to the high costs, sea experiments lack flexibility in their implementation.
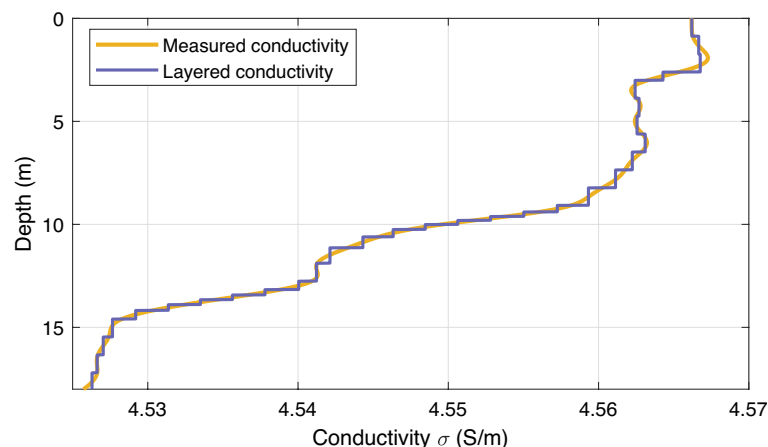

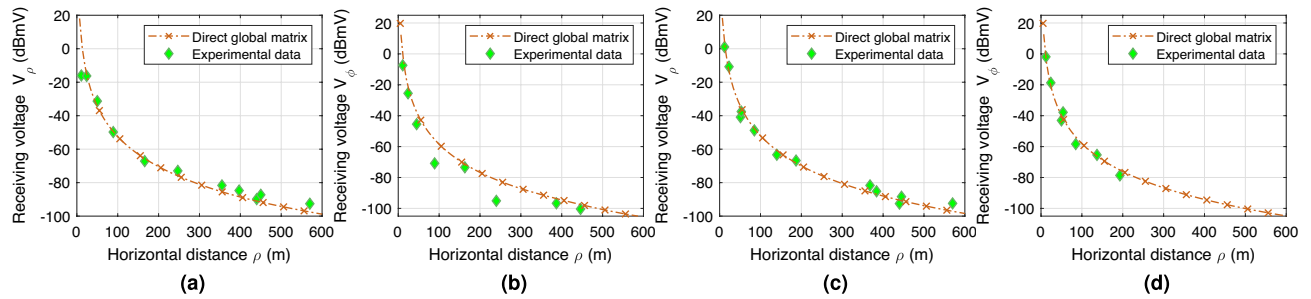**Figure 8.** Seawater conductivity along the vertical depth.

Figure 9. Comparison of theoretical and experimental results. (**a**) receiving voltage V_ρ in seawater, (**b**) receiving voltage V_φ in seawater, (**c**) receiving voltage V_ρ in air, (**d**) receiving voltage V_φ in air.

Numerical experiments

To overcome the limitations of numerical simulations and sea experiments, we introduced the more realistic EM parameter profiles in the N-layered media model. In this section, the conductivity and relative permittivity of seawater will be obtained based on the existing marine environment parameter database. Typical EM parameter profiles of seawater are selected to establish numerical models of EM wave propagation in non-homogeneous seawater. Then, combined with the solution method of the multi-layer propagation model in this paper, the EM field generated by the underwater HMD is obtained. The impact of changes in seawater EM parameters on the propagation performance of EM waves was evaluated and analyzed through numerical simulation.

Conductivity of seawater

Although some databases of ocean conductivity profiles currently exist, in order to ensure the synchronization of conductivity and permittivity, this article will use the marine environment database as the common initial condition. The calculation method for conductivity is as follows:

$$\sigma(S, T, P) = \sigma(35, 15, 0 \text{ dbar})R \tag{8}$$

where S is the salinity, T is the temperature, P is the pressure, and the reference conductivity is the $\sigma(35, 15, 0 \text{ dbar}) = 4.2914(\text{S/m})$, and the calculation method of the conductivity ratio R can be obtained from TEOS-10[19].

Combining Eq. (8) and the ocean environment dataset, we can get the temporal mean of ocean conductivity data. The marine environmental parameters required for the calculation can be obtained from the World Ocean Atlas (WOA) . This data set is a collection of objectively analyzed, quality-controlled temperature, salinity et al. based on profile data from the World Ocean Database (WOD).

It is illustrated in Fig. 10 that the conductivity of seawater at all depth layers shows a trend of being high near the equator and low at the poles, which is roughly the same as the distribution of temperature. And as the depth increases, the conductivity gradually decreases. Moreover, compared with the horizontal range, the change in seawater conductivity in the vertical direction is more dramatic.
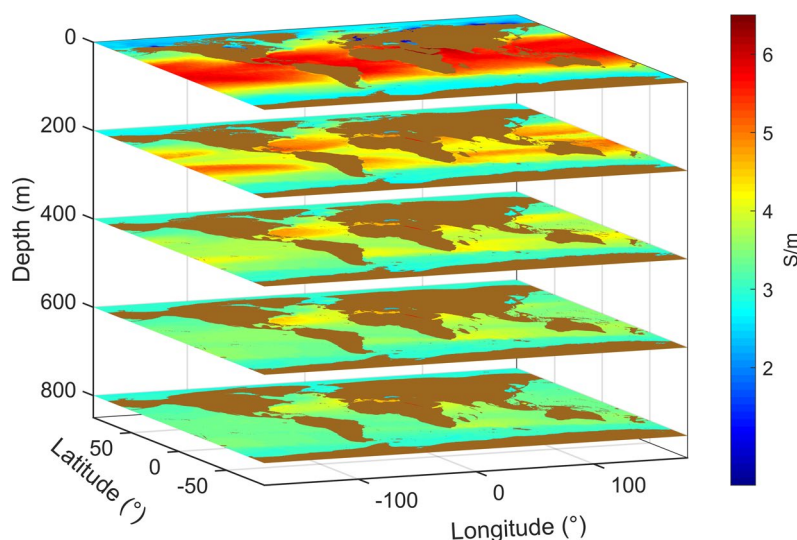

Figure 10. Conductivity profile and the number of layers in seawater.

Relative permittivity of seawater

The complex relative permittivity of seawater can be represented by the empirical formula[31]:

$$\varepsilon(T, S) = \varepsilon_\infty + \frac{\varepsilon_s(T, S) - \varepsilon_\infty}{1 - (i\omega\tau(T, S))^{1-\eta}} + i\frac{\sigma}{\omega\varepsilon_0} \tag{9}$$

where ε_∞ is the relative permittivity at infinite frequency, ε_s is the static permittivity, τ is the relaxation time in seconds, η is an empirical parameter that describes the distribution of relaxation times, and the conductivity σ can be obtained by Eq. (8).

Figure 11 shows the variation curve of relative permittivity with frequency at different temperatures and salinities. It is illustrated in Fig. 11 that when the frequency is less than 1 MHz, the real part of the permittivity basically doesn't change with the frequency. But the imaginary part changes greatly, which is caused by the conductivity of seawater. And the real part of permittivity is inversely related to temperature and salinity, while the imaginary part is the opposite.

Similar to conductivity, the temporal mean of global ocean relative permittivity is obtained at the frequency $f = 10$ kHz. It is illustrated in Fig. 12a that the real part of the relative permittivity near the equator is smaller than that at the poles. However, the variation with depth near the equator is greater. This is mainly due to the lower amplitude and variation range of seawater temperature at the poles. Moreover, compared to the real part of the permittivity, the imaginary part has a wider range of variation, as shown in Fig. 12b.

Compare and analyze

In this subsection, the influence of non-homogeneous seawater on EM wave propagation is evaluated by numerical simulation. To ensure the applicability and usefulness of the results in real-world scenarios, the EM parameters of seawater are obtained by substituting the temperature, salinity, and depth data from the WOA database into
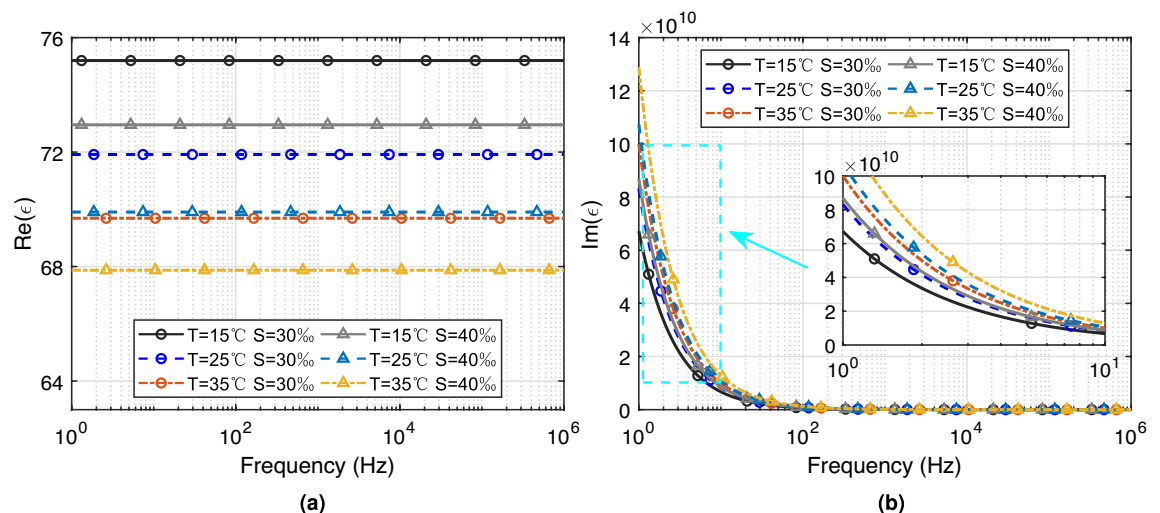

Figure 11. Complex relative permittivity of seawater at different temperatures and salinities. (**a**) Real part, (**b**) Imaginary part.
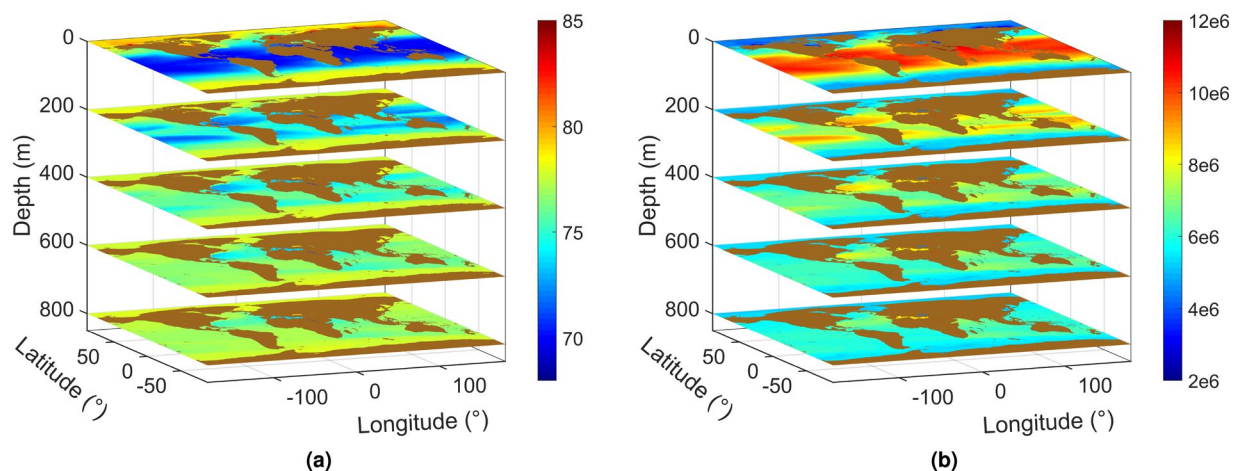

Figure 12. Global Ocean relative permittivity in June. (**a**) Real part, (**b**) Imaginary part.

Eqs. (8) and (9). The stratification of seawater corresponded to the standard depth divisions in the WOA database. The EM parameters of each layer are calculated by averaging the EM parameters at the upper and lower interfaces. Except for the conductivity and permittivity of seawater, all other parameters are the same as in Table 1.

Two typical profiles are selected for numerical simulation in Fig. 13. It is illustrated in Fig. 13a that the conductivity of Profile I is positively correlated with depth. Profile I showcases the characteristics of seawater EM parameters near polar regions and in the Black Sea. The surface temperature of the seawater near the poles is relatively low, while the deep seawater is connected to other sea areas and has a slightly higher temperature. Additionally, the melting of surface ice in polar regions dilutes the seawater, causing the salinity to increase with depth. The Black Sea is geographically closed, and the deep seawater lacks exchange, so the salinity increases with depth. Consequently, the conductivity of seawater in these areas increases with depth. While the conductivity of Profile II gradually decreases with increasing depth. And the conductivity of Profile II is overall higher than that of Profile I. As shown in Fig. 13b, the imaginary part of the relative permittivity has profiles similar to that of conductivity. Profile II exemplifies the seawater EM parameter distribution in most ocean areas, where temperature significantly decreases with increasing depth while salinity remains relatively stable. This leads to a reduction in seawater conductivity with depth.

It is illustrated in Fig. 14a,b that the variation range of field strength in Profile II is larger than that in Profile I. This is due to the fact that the attenuation constant of seawater is positively related to the conductivity and the imaginary part of the complex relative permittivity, and the average conductivity in profile II is relatively large. There is a shadow in Fig. 14a,b, which is caused by the interference of lateral waves from seawater-air path and seawater-seafloor path. The attenuation rate of field strength with depth can reach about 15 dB in this shadow. It is obvious in Fig. 14c,d that there is a triangular area below the shadow, where the attenuation rate with depth is positive. This means that lateral waves from the seawater-seafloor path contribute the main energy in this region. Similarly, the main energy of the EM wave above the shadow is the lateral wave from the seawater-air, and its attenuation rate is positively related to the conductivity of seawater. In addition, since the conductivity of seawater in Profile I is positively related to depth, lateral waves from above have less attenuation in seawater than those from below under the same propagation distance. Therefore, the area of the triangular region in Profile I is smaller than that in Profile II.

The phase of the EM field components is also one of the important parameters to evaluate the impact of non-constant EM parameters in seawater on EM wave propagation. It is illustrated in Figure 15 that the EM
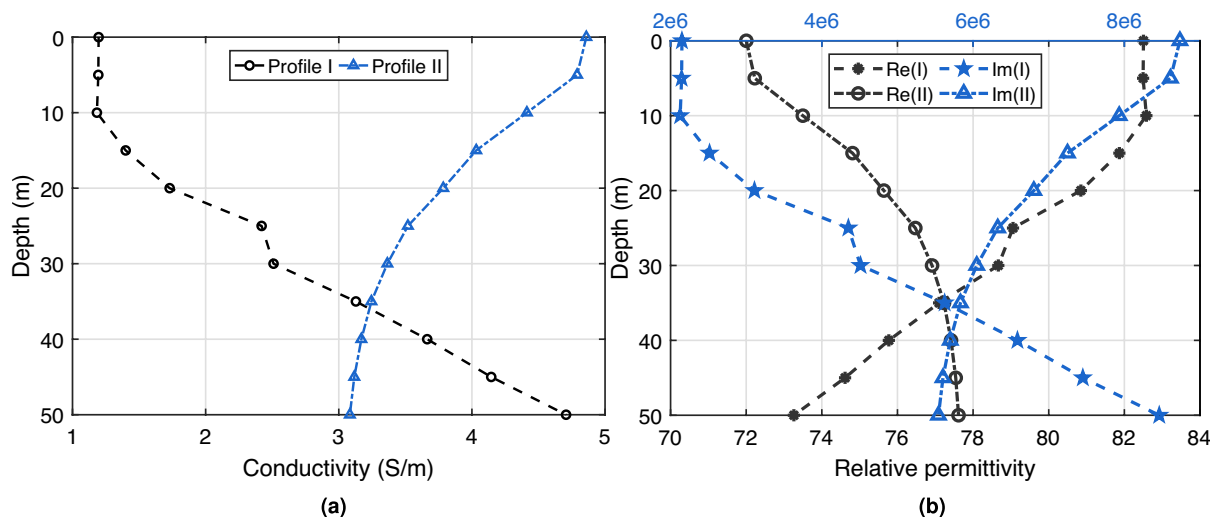

Figure 13. The typical profiles of EM parameters in the simulation, (**a**) Conductivity, (**b**) Complex relative permittivity at 10kHz.
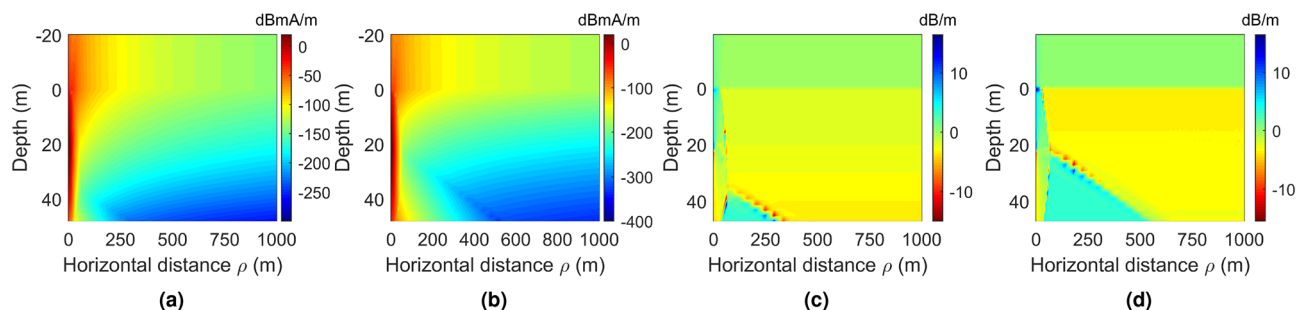

Figure 14. The vertical distribution of magnetic component H_φ, (**a**) the intensity in Profile I, (**b**) the intensity in Profile II, (**c**) the attenuation rate with depth in Profile I, (**d**) the attenuation rate with depth in Profile II.
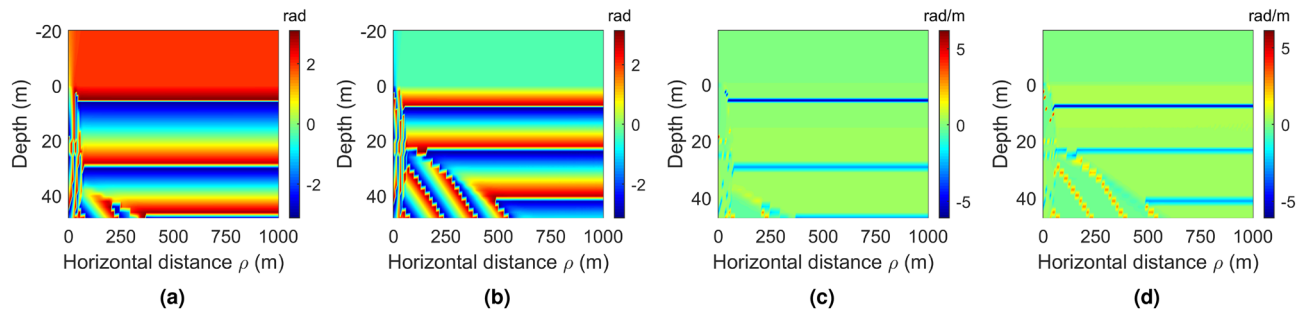
Figure 15. The vertical distribution of magnetic component H_φ, (**a**) the phase in Profile I, (**b**) the phase in Profile II, (**c**) the phase change rate with depth in Profile I, (**d**) the phase change rate with depth in Profile II.

parameters of seawater also affect the phase of the EM wave in the air, and the phase change of the EM field component in seawater is larger than that in the air. When the horizontal distance is far, the phase change rate of the H_φ in Profile I gradually increases with depth, but the phase is almost constant with horizontal distance. This phenomenon can be explained by the fact that the primary energy in that region is from the seawater-air path, and the wavelength of EM waves in the air is much longer than 1km. In the triangular area, the phase variation period in the horizontal distance is about 158m, which is the wavelength of EM waves on the seafloor. This once again confirms that the main energy of EM waves in this area is the lateral wave from the seawater-seafloor path.

Figure 16 shows the vertical distribution of EM field component intensity at different frequencies in two profiles. As the frequency increases, the absorption loss of EM waves in seawater and the seafloor gradually intensifies, while absorption loss is non-existent in air. Therefore, compared to the attenuation magnitude of lateral waves from the seawater-seafloor path, that from the seawater-air path with respect to frequency is smaller at the same location. As a result, the area where the lateral waves from the air are the main component gradually increases, and the shadow area gradually moves downward. This phenomenon is consistently observed in both profiles. And the variation range of intensity also becomes larger with the increase in frequency. The variation range of intensity in Profile I is much smaller than that in Profile II.

It is illustrated in Fig. 17 that the behavior of each EM component under different profiles is basically similar to H_φ. However, compared with the magnetic field component in air, the electric field component is more obviously affected by the EM parameter profile. It is illustrated in Fig. 17a,d that the electric field component E_ρ in the air first decreases and then increases with the receiving height. But the reduction in Profile I is much greater than that in Profile II. This should be caused by the changes in seawater EM parameters affecting the trapped surface waves.

In summary, the conductivity and permittivity of seawater are simulated and analyzed based on the existing marine environment database in this section. The EM field components in different EM parameter profiles were simulated through numerical methods. The results show that the non-uniformity of seawater not only affects the underwater EM field but also affects the EM field in the air. The influence is mainly reflected in the amplitude, phase, change rate, and spatial distribution. The electric components are more widely affected than the magnetic components.
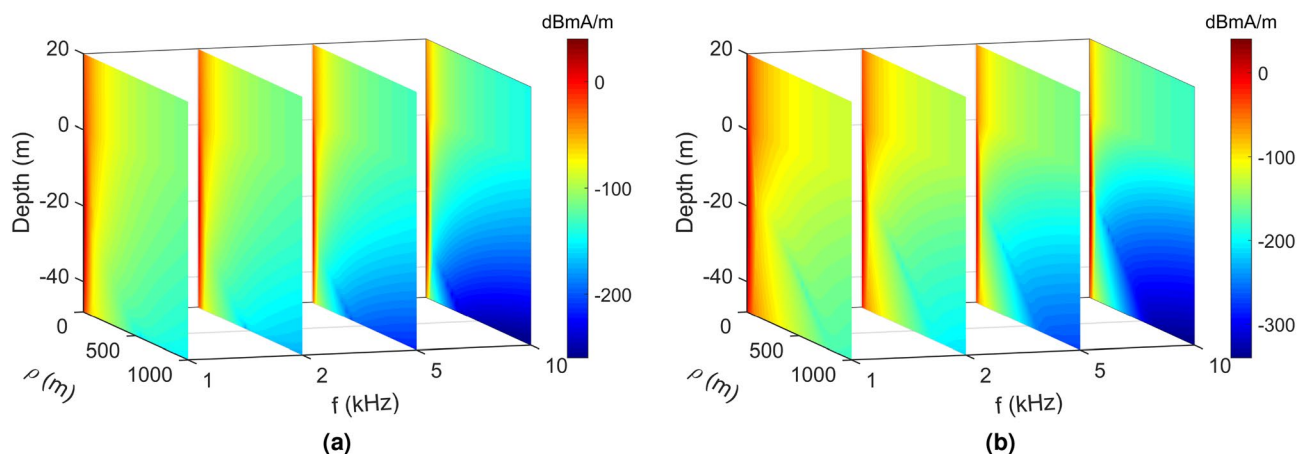

Figure 16. The vertical distribution of magnetic component H_φ intensity at different frequencies, (**a**) Profile I, (**b**) Profile II.
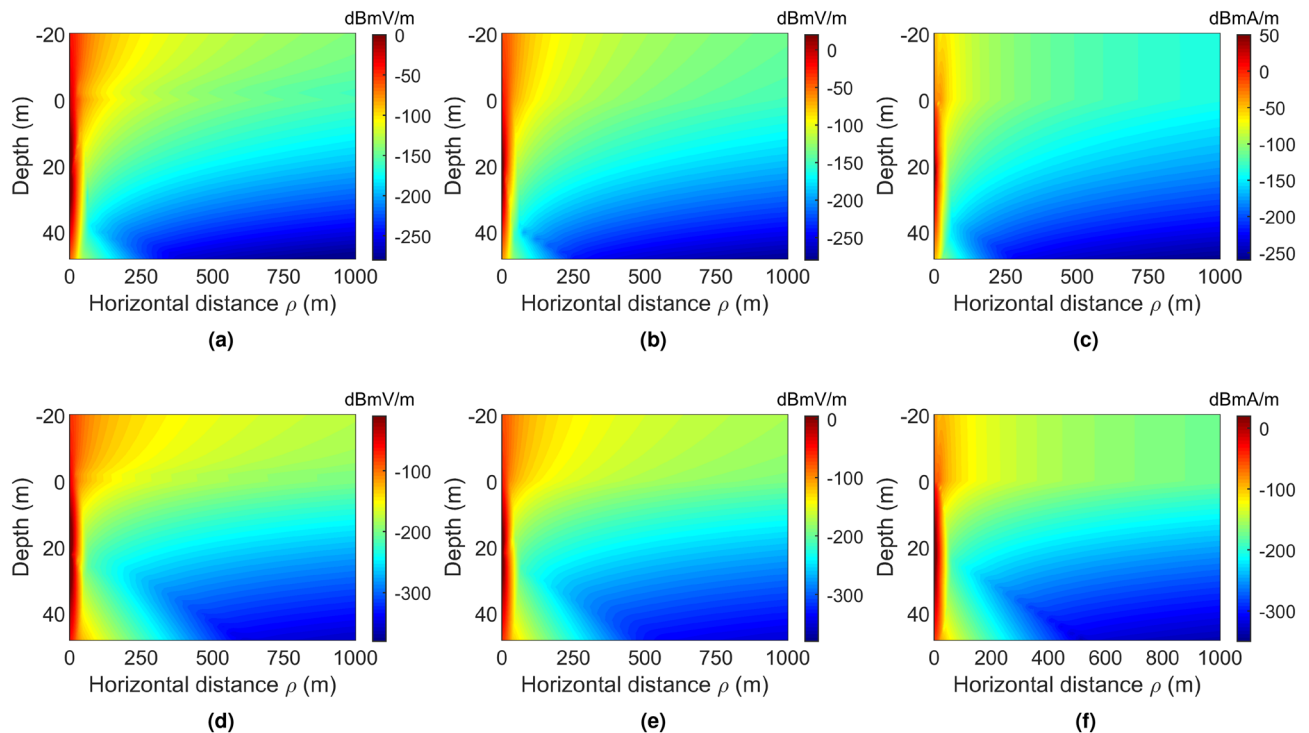
Figure 17. The vertical distribution of different EM field components intensity, (**a**) E_ρ in Profile I, (**b**) E_φ in Profile I, (**c**) H_ρ in Profile I, (**d**) E_ρ in Profile II, (**e**) E_φ in Profile II, (**f**) H_ρ in Profile II.

Conclusions

In this paper, a numerical model of EM wave propagation in non-homogeneous seawater is presented. A direct global matrix approach is proposed to solve the N-layered media model, whose computational accuracy is not affected by the number of layers. The necessity and correctness of the model and method are verified through numerical simulations and sea experiments. Combined with the existing marine environment database, the impact of non-homogeneous seawater on EM wave propagation performance is comparatively analyzed through numerical experiments. The results show that the non-uniformity of seawater has a great influence on the intensity, phase, change rate, and spatial distribution of EM waves. This effect increases with frequency. The behavior of each underwater EM component is basically similar. But the electrical components near the sea surface in the air are more severely affected by non-homogeneous seawater than the magnetic components.

Research on EM wave propagation in non-homogeneous seawater in this paper will be meaningful for EM communications and detection in the practical marine environment. In addition, the model and method in this paper can be used for other types of underwater radiation sources and can also be applied to solve the propagation of EM waves in other multi-layer media, such as multi-layer ice in the polar regions.

Data availability

For the data used or generated during the study, please contact the corresponding author.

References

1. Wang, C., Cui, Y., Song, X., Zhang, Y. & Yuan, Z. A novel underwater target detection method based on low-frequency magnetic signal generated by portable transmitter. *IEEE Sens. J.* **23**, 8459–8465. https://doi.org/10.1109/JSEN.2023.3253708 (2023).
2. Purkis, S. & Chirayath, V. Remote sensing the ocean biosphere. *Annu. Rev. Environ. Resour.* **47**, 823–847. https://doi.org/10.1146/annurev-environ-112420-013219 (2022).
3. Pei, J. *et al.* A sea clutter suppression method based on machine learning approach for marine surveillance radar. *IEEE J. Sel. Top. Appl. Earth Observ. Remote Sens.* **15**, 3120–3130. https://doi.org/10.1109/JSTARS.2022.3167410 (2022).
4. Ma, Y., Zhang, Q. & Wang, H. 6g: Ubiquitously extending to the vast underwater world of the oceans. *Engineering* **8**, 12–17. https://doi.org/10.1016/j.eng.2021.07.017 (2022).
5. Tian, Y. *et al.* Modeling and simulation on three-layer media propagation characteristics of underwater electromagnetic field in shallow sea area, in *2019 IEEE 4th Advanced Information Technology, Electronic and Automation Control Conference (IAEAC)*, 1515–1518 https://doi.org/10.1109/IAEAC47372.2019.8997918 (2019).
6. Yang, S. *et al.* Long-range em communication underwater with ultracompact elf magneto-mechanical antenna. *IEEE Trans. Antennas Propag.* **71**, 2082–2097. https://doi.org/10.1109/TAP.2022.3227799 (2023).
7. Ren, Y., Wang, H. & Yang, K. Efficient method for solving underwater electromagnetic fields generated by radiation sources in seawater. *IEEE Antennas Wirel. Propag. Lett.* **23**, 1638–1642. https://doi.org/10.1109/LAWP.2024.3364772 (2024).

8. Quintana-Díaz, G. *et al.* Underwater electromagnetic sensor networks-part i: Link characterization. *Sensors* **17**, 189. https://doi.org/10.3390/s17010189 (2022).
9. Smolyaninov, I., Balzano, Q. & Young, D. Development of broadband underwater radio communication for application in unmanned underwater vehicles. *J. Mar. Sci. Eng.* **8**, 370. https://doi.org/10.3390/jmse8050370 (2020).
10. Xu, H., Gu, T. & Li, K. Approximated solutions for elf near-field propagation due to a horizontal electric dipole excitation near the sea-rock boundary. *IEEE Trans. Antennas Propag.* **66**, 2471–2481. https://doi.org/10.1109/TAP.2018.2810328 (2018).
11. Wang, H., Yang, K. & Yang, Y. Electromagnetic fields in air produced by underwater magnetic dipoles with attitude variation in real marine environment. *J. Electromagn. Waves Appl.* **33**, 1978–1995. https://doi.org/10.1080/09205071.2019.1661288 (2019).
12. Weng, A.-H., Liu, Y.-H., Yin, C.-C. & Jia, D.-Y. Singularity-free green's function for em sources embedded in a stratified medium. *Appl. Geophys.* **13**, 25–36. https://doi.org/10.1007/s11770-016-0549-x (2016).
13. Nie, Z., Wang, S., Chen, D. & Deng, T. Seabed-rock-layer electromagnetic communication channel model with low path loss based on evanescent wave. *Radioengineering* **27**, 431–439 (2018) (**10.13164/re.2018.0431**).
14. Kawamura, T. *et al.* Experimental observation of lateral waves propagation along seabed, in *2023 IEEE International Symposium on Antennas and Propagation and USNC-URSI Radio Science Meeting (USNC-URSI)*, 273–274, https://doi.org/10.1109/USNC-URSI52151.2023.10238122 (2023).
15. Le Vine, D., Zhou, Y. & Lang, R. Model for dielectric constant of seawater based on l-band measurements with conductivity by definition. *IEEE Geosci. Remote Sens. Lett.* **19**, 1–5. https://doi.org/10.1109/LGRS.2022.3221888 (2022).
16. Boutin, J. *et al.* New seawater dielectric constant parametrization and application to SMOS retrieved salinity. *IEEE Trans. Geosci. Remote Sens.* **61**, 1–13. https://doi.org/10.1109/TGRS.2023.3257923 (2023).
17. Ishtaiwi, M., Hajjyahya, M. & Habbash, S. Electrical properties of dead sea water. *J. Appl. Math. Phys.* **9**, 3094–3101. https://doi.org/10.4236/jamp.2021.912201 (2021).
18. Rezaei-Latifi, A. Spatial and temporal variability of the surface permittivity of Persian gulf water at the c-band. *Appl. Math. Model.* **40**, 1069–1081. https://doi.org/10.3390/s17010189 (2016).
19. McDougall, T. *et al.* The international thermodynamic equation of seawater 2010 (teos-10): Calculation and use of thermodynamic properties. *Glob. Ship-Based Repeat Hydrogr. Man. IOCCP Rep. No* **14** (2009).
20. Tyler, R., Boyer, T., Minami, T., Zweng, M. & Reagan, J. Electrical conductivity of the global ocean. *Earth Planets Space* **69**, 156. https://doi.org/10.1186/s40623-017-0739-7 (2017).
21. Zheng, Z. *et al.* Three-stage vertical distribution of seawater conductivity. *Sci. Rep.* **8**, 9916. https://doi.org/10.1038/s41598-018-27931-y (2018).
22. Chakraborty, U., Tewary, T. & Chatterjee, R. P. Exploiting the loss-frequency relationship using rf communication in underwater communication networks, in *2009 4th International Conference on Computers and Devices for Communication (CODEC)*, 1–4 (2009).
23. Qureshi, U. *et al.* Rf path and absorption loss estimation for underwater wireless sensor networks in different water environments. *Sensors* **16**, 890. https://doi.org/10.3390/s16060890 (2016).
24. Saini, P., Singh, R. & Sinha, A. Path loss analysis of rf waves for underwater wireless sensor networks, in *2017 International Conference on Computing and Communication Technologies for Smart Nation (IC3TSN)*, 104–108, https://doi.org/10.1109/IC3TSN.2017.8284460 (2017).
25. Tahir, M., Yan, P. & Shuo, L. Channel characterization of EM waves propagation at MHZ frequency through seawater. *Int. J. Commun. Syst.* **31**, e3462. https://doi.org/10.1002/dac.3462 (2018).
26. Wang, J. & Li, B. Electromagnetic fields generated above a shallow sea by a submerged horizontal electric dipole. *IEEE Trans. Antennas Propag.* **65**, 2707–2712. https://doi.org/10.1109/TAP.2017.2681320 (2017).
27. Kong, J. A. *Electromagnetic Wave Theory* 1st edn. (Wiley, 1986).
28. Hu, Y., Fang, Y., Wang, D., Zhong, Y. & Liu, Q. Electromagnetic waves in multilayered generalized anisotropic media. *IEEE Trans. Geosci. Remote Sens.* **56**, 5758–5766. https://doi.org/10.1109/TGRS.2018.2825430 (2018).
29. Jensen, F., Kuperman, W., Porter, M. & Schmidt, H. *Computational Ocean Acoustics* 2nd edn. (Springer, 2011).
30. Firouzeh, Z., Vandenbosch, G., Moini, R., Sadeghi, S. & Faraji-Dana, R. Efficient evaluation of green's functions for lossy half-space problems. *Prog. Electromag. Res.* **109**, 139–157. https://doi.org/10.2528/PIER10062310 (2010).
31. Somaraju, R. & Trumpf, J. Frequency, temperature and salinity variation of the permittivity of seawater. *IEEE Trans. Antennas Propag.* **54**, 3441–3448. https://doi.org/10.1109/TAP.2006.884290 (2006).

Acknowledgements

Author contributions

Conceptualization, Y.R.; methodology, Y.R.; investigation, K.Y.; writing–original draft preparation, Y.R.; writing–review and editing, H.W. and K.Y.; visualization, Y.R. and H.W.; supervision, H.W. and K.Y.; funding acquisition, H.W. and K.Y.. All authors have reviewed and agreed to the manuscript.

Competing interests

The authors declare no competing interests.

Additional information

Supplementary Information The online version contains supplementary material available at https://doi.org/10.1038/s41598-024-72036-4.

Correspondence and requests for materials should be addressed to H.W.

Reprints and permissions information is available at www.nature.com/reprints.

Publisher's note Springer Nature remains neutral with regard to jurisdictional claims in published maps and institutional affiliations.